Fatigue & Fracture of Engineering Materials & Structures

WILEY

FFEMS Fatigue & Fracture of Engineering Materials & Structures

ORIGINAL ARTICLE OPEN ACCESS

The Importance of Rubber Compounding Approach in Damage Evolution and Fatigue Performance of Carbon Nanotubes Doped Natural Rubber

Ali Esmaeili[1] | Deepak George[1] | Thomas Lake[1] | Lewis Tunnicliffe[2] | Ian Masters[1] | Mokarram Hossain[1]

[1]Zienkiewicz Institute for Modelling, Data and AI Faculty of Science and Engineering, Swansea University, Swansea, UK | [2]Birla Carbon, Marietta, Georgia, USA

Correspondence: Ali Esmaeili (ali.esmaeili@swansea.ac.uk)

Received: 4 March 2025 | **Revised:** 5 August 2025 | **Accepted:** 8 August 2025

Funding: This work was supported by the Birla Carbon (USA), EPSRC through the Supergen ORE Hub (EP/S000747/1), who have awarded funding for the Flexible Fund project Supergen ORE Hub Flexible Fund (FF2021-1036), EPSRC via a Standard Grant (EP/Z535710/1) and the Royal Society (UK) through the International Exchange Grant (IEC/NSFC/211316), Swansea Bay City Deal and the European Regional Development Fund through the Welsh European Funding Office and the Royal Society (UK) through the International Exchange Grant (IEC/NSFC/211316).

Keywords: carbon nanotubes | compounding technique | damage evolution | defect | fatigue life | natural rubber

ABSTRACT

This study was aimed to investigate the fatigue life of carbon nanotubes (CNTs) filled natural rubbers (NR) prepared by two different compounding techniques, including wet and dry methods. This was done to correlate the presence of defects to fatigue performance and to identify the optimum dispersion approach for CNTs/NR. The wet approach possessed a higher number of large defects compared to the dry approach, whereas the latter manifested better CNT dispersion. The presence of a higher number of large defects accounted for a significant reduction in the fatigue life in the wet batch with respect to dry samples. The formation of multiple tiny cracks and their further developments via crack shielding and crack coalescence were considered for damage evolution at the macroscale, while the presence of wrenching and river-like patterns was notable at the microscale. Ultimately, the dry approach could be a better compounding technique for CNT dispersion considering its high quasi-static and fatigue properties.

1 | Introduction

Natural rubber (NR) has extensively been used in various fields such as the tyre industry [1] and wave energy converters (WECs) [2, 3]. This indicates that NR has inherent quasi-static and good dynamic properties such as a high fatigue life. The latter is quite important, as most rubber applications operate under repeated (cyclic) loading conditions; therefore, a high fatigue life is required [4, 5]. Cyclic loadings applied to elastomers during their service lives can either result in the nucleation of tiny cracks within the bulk of materials or lead to the growth of existing defects, filler agglomerations or porosity, to complete failure over time.

In this context, carbon nanotubes (CNTs) have been widely used as a promising nano-reinforcement in rubbers to enhance their mechanical performance under static and dynamic conditions [6–13]. However, the resulting functional benefit is strongly dependent on the state of CNT dispersion and the existence of defects such as microscale voids and pores. It is worthy to note that regardless of the compounding techniques used, it is inevitable to make defect-free CNTs/NR nanocomposites; therefore, the optimization of compounding parameters is important. CNTs have high surface energy and large aspect ratio, so one of the existing challenges of NRs filled with CNTs is to achieve a proper CNT dispersion instead of creating agglomerations [14]. Hence, many efforts have been made to mitigate the CNTs bundling

Summary

- Damage evolution and fatigue life of CNTs filled NR prepared by dry and wet techniques.
- To correlate the presence of defects to mechanical and fatigue properties.
- To grasp crack initiation and crack growth in CNTs filled rubber during fatigue testing.
- High-quality digital image correlation results were provided to show the strain values.

such as latex mixing, solution methods, and mechanical/melting technology. Solution mixing was one of the few methods attempted for proper dispersions of CNTs into the NR [15–17] in which NR gum is dissolved into a compatible solvent (toluene or similar) followed by dispersion of CNTs within the NR/toluene liquid mixture. In a previous attempt made by the authors [4, 18], a novel combined solution method and two-roll mill was compared with the standard melt mixing technique in terms of the state of CNT dispersion and dynamic shear properties. It was shown that a combined approach can provide a better CNT dispersion with respect to the mechanical mixing, while no significant difference in dynamic shear properties was identified among the two methodologies used. However, this needs to be further investigated under more realistic test conditions including fatigue tests such that it can properly simulate the real working conditions under repeated loading scenarios.

Two different approaches have been used to investigate the fatigue life of rubbery materials that include crack nucleation and crack propagation approaches, which are based on continuum mechanics and fracture mechanics, respectively [19, 20]. Fatigue crack growth resistance of NR is based on the correlation of crack growth rate with respect to tearing energy and was extensively addressed in the literature [21–25], whereas fewer studies were conducted based on the crack nucleation approach in rubbers [8, 26–29]. To the best of the authors' knowledge, no study was performed to correlate the fatigue life of rubbers to the typical preexisting defects in NR, such as pores, assuming that it is inevitable to make CNT-NR nanocomposite materials with no defects. Therefore, damage evolution during fatigue tests is an important phenomenon requiring further studies in detail to grasp the crack nucleation process and its propagation. Although some studies discussed damage evolution in NR [27, 30, 31], it depends on the specimen geometry, test conditions, and materials tested. In addition, most of the previous studies focused mainly on achieving a good dispersion of CNTs in the NR matrix while neglecting the significant impact of preexisting voids on their dynamic properties. In fact, achieving a sound sample possessing ideal CNT dispersion and minimal voids and defects is challenging. Each compounding technique possesses its own advantages and disadvantages, such that some techniques lead to better CNT dispersion by sacrificing other characteristics, for instance, the presence of pores, and vice versa. Hence, the evaluation of damage development and the fatigue life of CNT-filled rubber prepared by different dispersion approaches can provide better estimation in regard to the performance of the dispersion approach used for CNTs.

Therefore, this study is aimed at comparing material characteristics, including the state of CNT dispersion and the presence of preexisting defects such as voids, and the fatigue life of the NR filled with CNTs prepared by two different compounding methods. Optical microscopy, SEM, and TEM were employed for materials characterization, while tensile and fatigue tests were conducted for the mechanical characterization. Macro- and microdamage evolutions throughout fatigue tests were discussed to identify crack propagation mechanisms, in order to correlate the presence of defects including voids and aggregations of CNTs with their fatigue performance and to find out the optimum dispersion approach for CNTs/NR compounding.

2 | Experiment

2.1 | Materials and Sample Preparations

NR, SMR CV60 gum, and multiwall carbon nanotubes (MWCNTs) were provided by *Malaysian rubber* and *Nanocyl* companies, respectively. Two different dispersion techniques were employed that include solution mixing and a melting methodology known as mechanical mixing. The first technique, which is achieved by dissolving NR gum into toluene and sonication of the CNTs/toluene mixture followed by the addition of the CNTs/toluene mixture to the NR/toluene liquid mixture, is called the wet method. The second was performed in a dried state only, i.e., CNTs were added to the internal mixer directly, hereinafter called the dry method; 3-phr (parts per hundred rubber) CNTs loading was used for both approaches to mainly concentrate on the effects of CNTs dispersion and subsequent macro- and microstructural defects that can affect the fatigue life of NR. Zinc oxide (5 phr), stearic acid (2 phr), 6PPD (3 phr), and Sasol wax (2 phr) were incorporated into the rubber inside the internal mixer while sulfur (1.5 phr) and CBS (1.5 phr) were added on the two-roll mill. Further explanations regarding the dispersion and compounding techniques can be found in refs [4, 18].

2.2 | Material Characterizations

2.2.1 | Microscopy

The *ZEISS Smartzoom 5* digital light microscope was employed for analyzing surface defects including voids and cracks before and after the fatigue tests, while a Scanning Electron Microscope (SEM, *Zeiss Evo LS25*) was employed for fractography. Samples were coated by platinum to avoid electrostatic charging. Transmission Electron Microscopy (TEM), *Jeol JEM-1400* fitted with a Gatan Rio16 digital camera operated at 120 kV, was used to characterize the state of CNTs depression within the NR by preparing an ultrathin section of sample (60–70 nm) cut by an ultra-microtome at −120°C.

2.2.2 | Mechanical Testing

A highly advanced and custom-built electromechanical fatigue testing machine (*ADMET eXpert 8000, USA*) was used for the

tensile and fatigue tests (Figure 1a,b). A digital image correlation (DIC) system equipped with a 5.0 Megapixel digital camera (2448×2028 @ 75 fps) and a 2D DIC system analysis software were used for real-time reading of nominal strain throughout the test using a virtual extensometer and for further postprocessing of the images to obtain full-field planar strains (Figure 1c). A fine speckle was created over the surface of the samples using a roller stamp. Tensile properties of the nanocomposite rubbers were investigated by performing quasi-static tests up to 363% strain with a crosshead speed of 0.5 mm/s. The loading–unloading of the first 5 cycles during the quasi-static test were provided so that the Mullins effect as well as mechanical properties at the stable region can be observed. A sinusoidal waveform with a 2-Hz frequency was utilized for the fatigue tests. Different strain amplitudes including 48%, 97%, 144%, and 202% strains were used for the fatigue tests while an R-ratio of 0.1 (minimum to maximum strain ratio) was considered for all tests. At least six samples were tested for each batch for the fatigue tests, in which samples were tested simultaneously in one setup as shown in Figure 1a,b. It is worth noting that 12 samples were tested simultaneously, i.e., two sets of six where each set is taken from an individual batch. The cycle numbers to failure for each sample were obtained by postprocessing the load–displacement data. A dog bone sample was used for the fatigue tests, where the samples were cut from the molded rubber sheets with a 2-mm thickness by a standard die cutter according to ISO 37-type 2. It is worth noting that the longitudinal axis of the dog bone samples was collinear with the two-roll mill direction. The fatigue life of

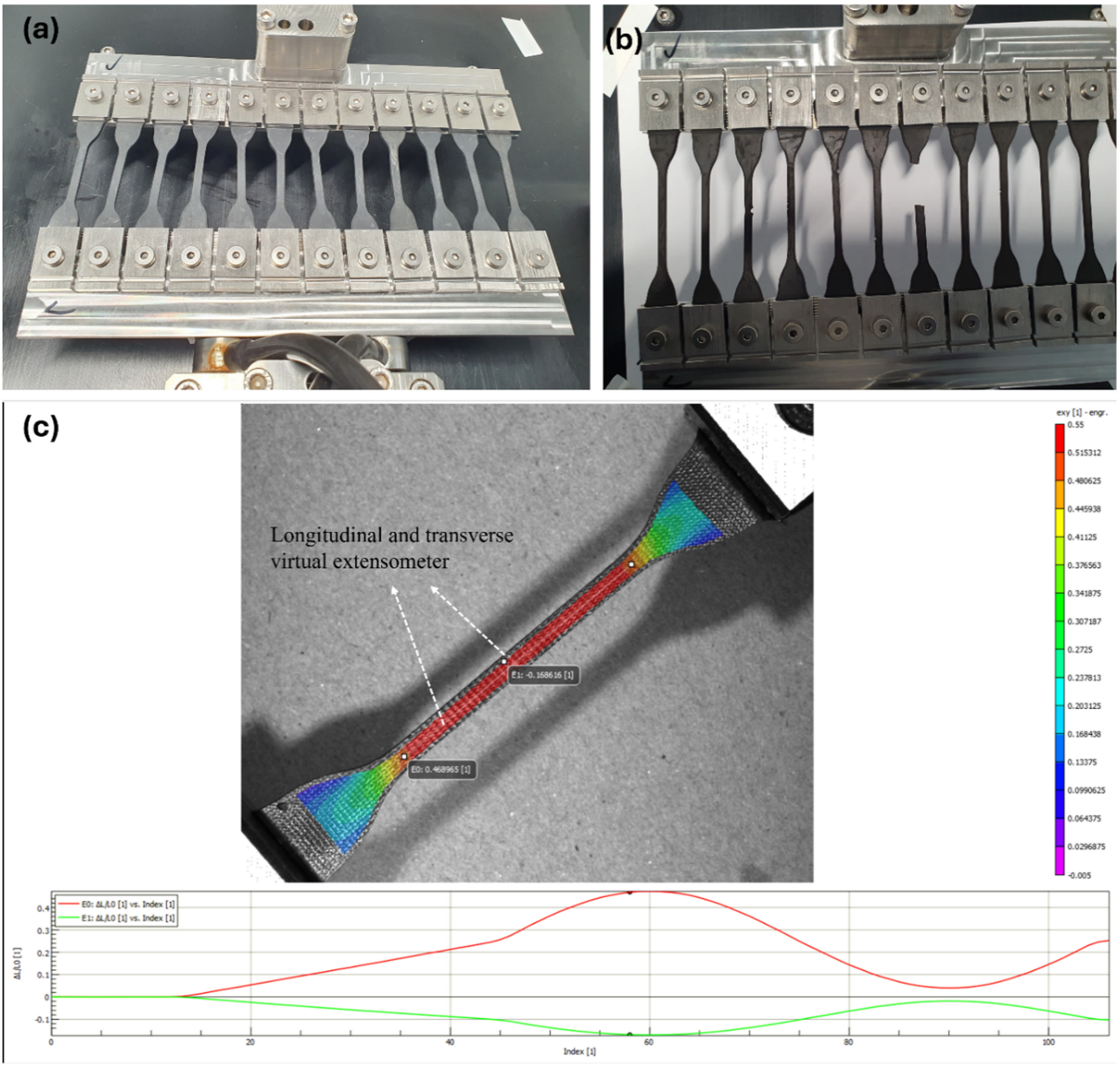

FIGURE 1 | Experimental fatigue test setup: (a,b) samples layout before and during fatigue testing, (c) full-field 2D strain within the surface of dog bon sample tested at approximately 48% strain. The red and green curves represent the longitudinal and transverse strains, respectively. [Colour figure can be viewed at wileyonlinelibrary.com]

the materials was counted from the start to the final rupture of each sample, i.e., a crack nucleation approach, which is based on continuum mechanics, was used in the current study [32]. Temperature variations throughout the fatigue tests were less than 4°C, which were measured by means of an infrared thermometer. This can be attributed to the small thickness of the samples (2 mm) used in this study, avoiding high heat build-up during the cyclic test [29, 33].

3 | Results and Discussion

3.1 | Microstructural Characterization

The presence of macro- and microscopic defects, especially voids, are common features observed in NR nanocomposite throughout mixing, curing, molding, or even preparation of test coupons for rubber testing [34]. In particular, for the solution mixing technique, due to the presence of residual solvent upon vulcanization, many voids or pin-hole defects can be seen [35]. In addition, achieving proper CNT dispersion is critical to effectively exploit reinforcement effects of CNTs in tailoring mechanical and electromechanical properties. One should make a balance between these two phenomena, i.e., proper CNT dispersion and the presence of voids, which are dependent on the compounding approaches used. It is worth noting that the crack initiation during fatigue tests mostly takes place as a result of preexisting defects acting as crack nucleation sites, even in virgin samples, which can be either surface or subsurface defects [20, 31]. Therefore, in general, the fewer the number of flaws, the higher the fatigue life. There are several reasons for the presence of such flaws in the filled NR, including filler agglomerations (CNTs for the current study), compounding processes, rubber formulations, i.e., additives, imperfections in the mold surfaces and mold release agents, and any other inclusions or contaminations throughout the compounding process [31, 36]. In this context, a comprehensive investigation in terms of the presence of preexisting defects, such as voids, cavities, and microcracks, along with the dispersion state of CNTs, is performed throughout this section using visual inspection, optical microscopy, and TEM. This helps better to distinguish the effects of different compounding techniques on achieving sound samples and correlates it to the observed fatigue properties.

3.1.1 | Optical Microscopy

Figure 2 shows the microscopic optical images of the cross section of pristine samples, extracted by a die cutter. The presence of voids varied in the range of a few microns to a couple of hundred microns and is noticeable for both compounding techniques. However, the wet approach manifests a relatively higher number of large voids, as highlighted by red arrows in Figure 2b, and a higher surface roughness compared to the dry one. This can be attributed to a higher amount of entrapped air in the wet sample, resulting from toluene used in wet samples, during processing and compression molding [36]. In this context, Sriring et al. [37] pointed out breaking up of nonrubber network structures on rubber particles at boundaries. Further, hydrophilic proteins and phospholipids, which are not insoluble in toluene, and substituting them by randomly dispersed aggregated nonrubber particles within rubber matrix, can be accounted for the void formation. This could be the reason for the presence of higher defects and surface roughness for the wet samples prepared by solution methods as shown in Figure 2b in which the observed defects randomly distributed and manifesting a more likely irregular shape.

3.1.2 | TEM Analysis

TEM images of the nanocomposites are shown in Figure 3 indicating a relatively better dispersion state of CNTs in the wet method compared to the dry technique. Moreover, the presence of CNT agglomeration is notable in the dry method, as shown by the yellow arrow in Figure 3a accompanied by a CNT-poor region, as highlighted by the red arrow. In contrast, the wet sample manifests a more homogeneous CNT dispersion. This can be attributed to the solution method assisted by bath sonication used for this sample. It is also worth noting that the wet sample manifested a higher electrical conductivity, as reported in our previous study [4], relatively two orders of magnitude, with

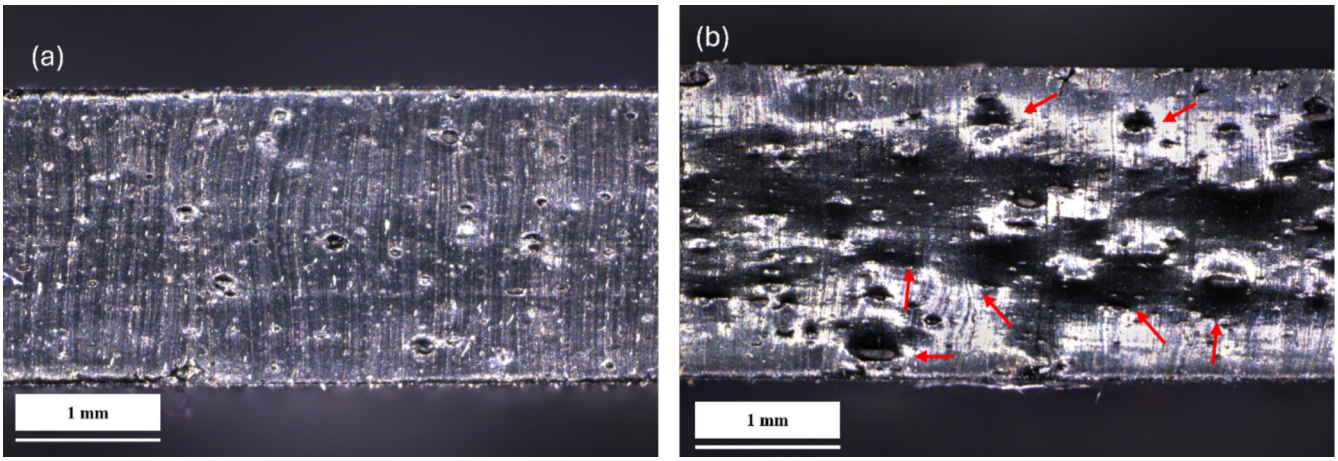

FIGURE 2 | Optical image of the cross section of virgin samples cut by dog bone cutter manifesting presences of voids: (a) 3-phr dry, (b) 3-phr wet possessing higher number of voids compared to dry one highlighted by red arrows. The magnification is 78 X. [Colour figure can be viewed at wileyonlinelibrary.com]

respect to the one prepared by the dry method, which is in agreement with the TEM results [4].

3.2 | Mechanical Characterization

Mechanical properties will be studied in this section to explore the quasi-static and fatigue properties.

3.2.1 | Mullins Effect

Figure 4 shows stress–strain curves up to 363% strain for five consecutive cycles in which the fifth cycle of both samples showing more stabilized behavior is plotted separately in Figure 4b. It is worth noting that the maximum strain tested in this study was 363% due to constraints in applying the maximum displacement in the machine used. Mullins effect and permanent set can be seen for both samples, which can be related to the breakage of CNT networks as well as CNTs/rubber interactions [38], though no significant difference in the hysteresis can be seen for both wet and dry samples. This can be attributed to the same CNTs content used. In addition, 3-phr wet samples manifest slightly higher mechanical properties with respect to the dry method which can be related to better CNT dispersion resulting in proper interfacial shear load transfer between CNTs and rubber matrix and vice versa. This indicates that the presence of higher defects in the wet approach does not have a significant impact on the quasi-static properties at relatively low to medium strains.

3.2.2 | Fatigue Properties

Figure 5 summarizes fatigue test results performed at different strain amplitudes including all experimental fatigue data (unfilled circles and squares for wet and dry samples, respectively), average fatigue life (black filled circles and black filled squares for wet and dry samples, respectively), standard deviations, and fitted S-N curves. It clearly depicts that increasing the strain amplitude substantially reduces the fatigue life especially from 48% to 97% strains. A maximum average fatigue life of 1.58 and 1.09 million cycles for dry and wet samples, respectively, are achieved at 48% strain, whereas an average fatigue life of 0.24 and 0.13 million cycles for dry and wet, respectively, are reached at 97% strain manifesting transition from a high cyclic to a low cyclic region. Similarly, less variations can be seen for higher strains compared to low strains. This can be attributed

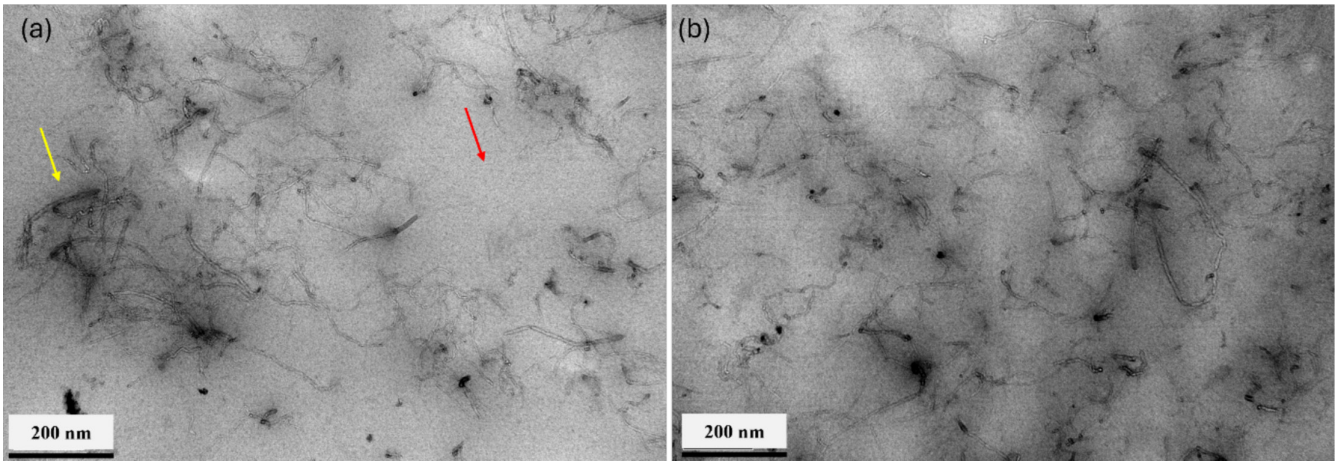

FIGURE 3 | CNTs dispersion within the NR matrix: (a) dry method, (b) wet approach. The scale for both pictures is 200 nm and the images are taken at 100,000 magnifications. Yellow and red arrows highlight CNTs agglomeration and CNTs-poor region respectively. [Colour figure can be viewed at wileyonlinelibrary.com]

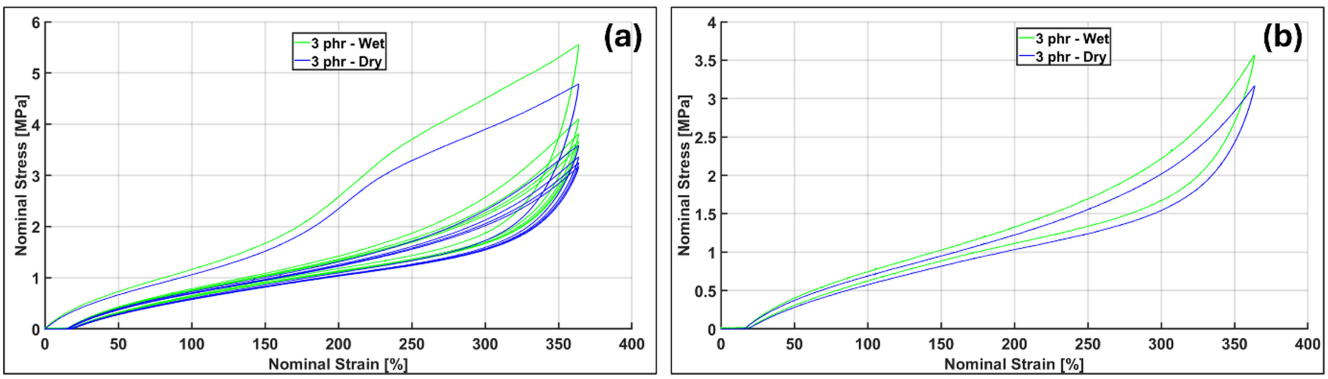

FIGURE 4 | Stress–strain curve of wet and dry samples subjected loading–unloading up to 363% strain: (a) presence of Mullins effect and permanent set, (b) fifth cycle manifesting a stabilized behavior. [Colour figure can be viewed at wileyonlinelibrary.com]

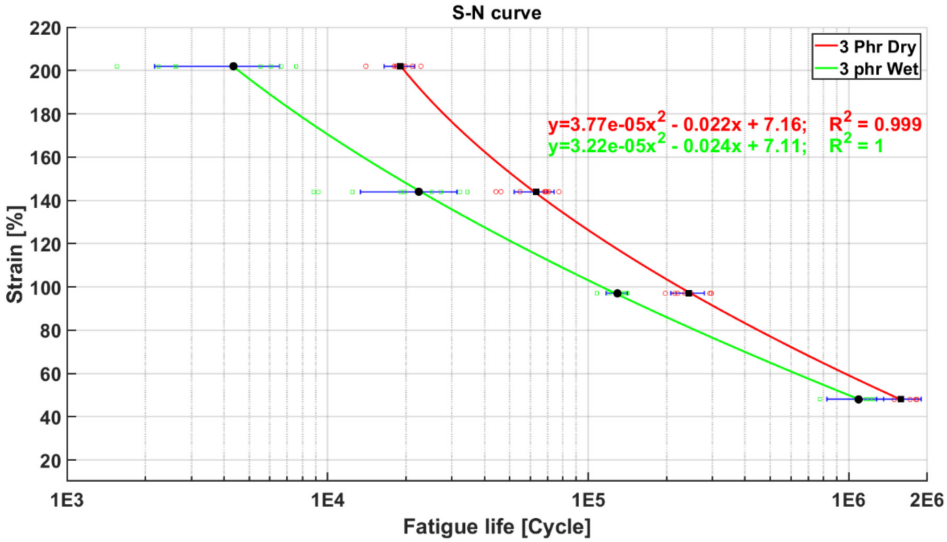

FIGURE 5 | Comparison of fatigue life of the natural rubber nanocomposite containing 3-phr CNTs prepared by wet and dry techniques. [Colour figure can be viewed at wileyonlinelibrary.com]

to a higher detrimental effect of defects at higher strains such that any macrodefect mitigates crack initiation and propagation resulting in premature critical failures. It can be concluded that the variations observed can be directly related to density and initial flaw size over the gauge length of the dog bone samples [31].

Furthermore, dry samples manifest significantly higher fatigue life with respect to wet ones as shown in Figure 5, while the latter demonstrates relatively better quasi-static properties with respect to former, resulting from proper CNTs dispersion. The lower fatigue life in wet samples can be related to the presence of higher defects, as shown by red arrows in Figure 2b, as well as the presence of randomly dispersed aggregated nonrubber particles within the rubber matrix, as discussed in s Section 3.1.1. Indeed, the occurrence of a relatively higher number of large defects, including voids in the wet batch, plays a significant role in degrading the dynamic properties of NR with respect to the agglomeration of CNTs observed in the dry batch. In other words, the presence of voids predominates the adverse effects of CNTs aggregation on the fatigue life of NR during repeated loading conditions; however, this is not the case for quasi-static conditions. This is mostly due to the size of initial flaws in the virgin wet specimen, as they are larger than flaws in dry specimens. Furthermore, the standard deviation of the results is higher for the wet method. This likely reflects a greater inhomogeneity in the sample in terms of defects/crack precursors, which is consistent with the microscopy images and fatigue results [39] .

It is vivid from the results that the dry method can be a better approach than the wet technique in terms of quasi-static and fatigue properties of NR, in addition to environmental concerns of using solvent, cost reduction, and preparation time. It is worth noting that toluene is considered a *volatile organic compound (VOC)*, which can contribute to air pollution through increasing ground level O_3 in the atmosphere, as well as posing a health hazard [40]. Comparison of quasi-static and fatigue results, as shown in Figures 4 and 5, indicates that although there is a slight difference in stress–strain behavior between the wet and the dry compounds, overall, the stress–strain behavior is quite similar (up to 363% strain). This is quite important since the results of strain-controlled fatigue tests are strongly dependent on the stiffness of compounds and the resulting strain energy density at maximum extension available to drive crack growth. Therefore, because two materials of similar stiffness were compared in this study, the fatigue life results better reflect the fundamental crack nucleation and growth differences between the compounds [41].

Figure 6 shows 2D principal strain distribution at the peak location for each strain amplitude. Readers are advised to refer to the videos of DIC results provided in Supporting Information for better visualization of the strain field distribution during the fatigue tests. A uniform strain distribution is achieved on the gauge region showing maximum nominal strain approximately equal to 48%, 97%, 144%, and 202%. It is worth noting that values of local strain distribution are relatively different with the strains obtain by the virtual extensometer, which can be related to slight misalignments of X- and Y-axis of the camera and dog bone samples; therefore, readers are advised to refer to values obtained by the virtual extensometer for a correct reading.

Figure 7a–d shows minimum strains corresponding to the minimum displacement at 48%, 97%, 144%, and 202% respectively. It is worth noting that a positive R-ratio (minimum to maximum strain ratio), in the range of 0.06 to 0.08 was applied for all fatigue tests performed (Figures 6 and 7) indicating nonrelaxing test conditions for all of them; thus, strain-induced crystallization (SIC) is dominant for all specimens during the fatigue tests [30]. It is worth noting that obtaining strain field using a DIC at ultra-large deformation (strain > 100%) is quite challenging with such a small sample, which was successfully obtained in this study by making the speckle patterns in two steps, i.e., on unstretched (relaxed sample) and 100%-stretched specimens. To the best of authors' knowledge, no study reported measuring strain at such large strains using DIC considering small width of the field of interest, i.e., 4 mm.

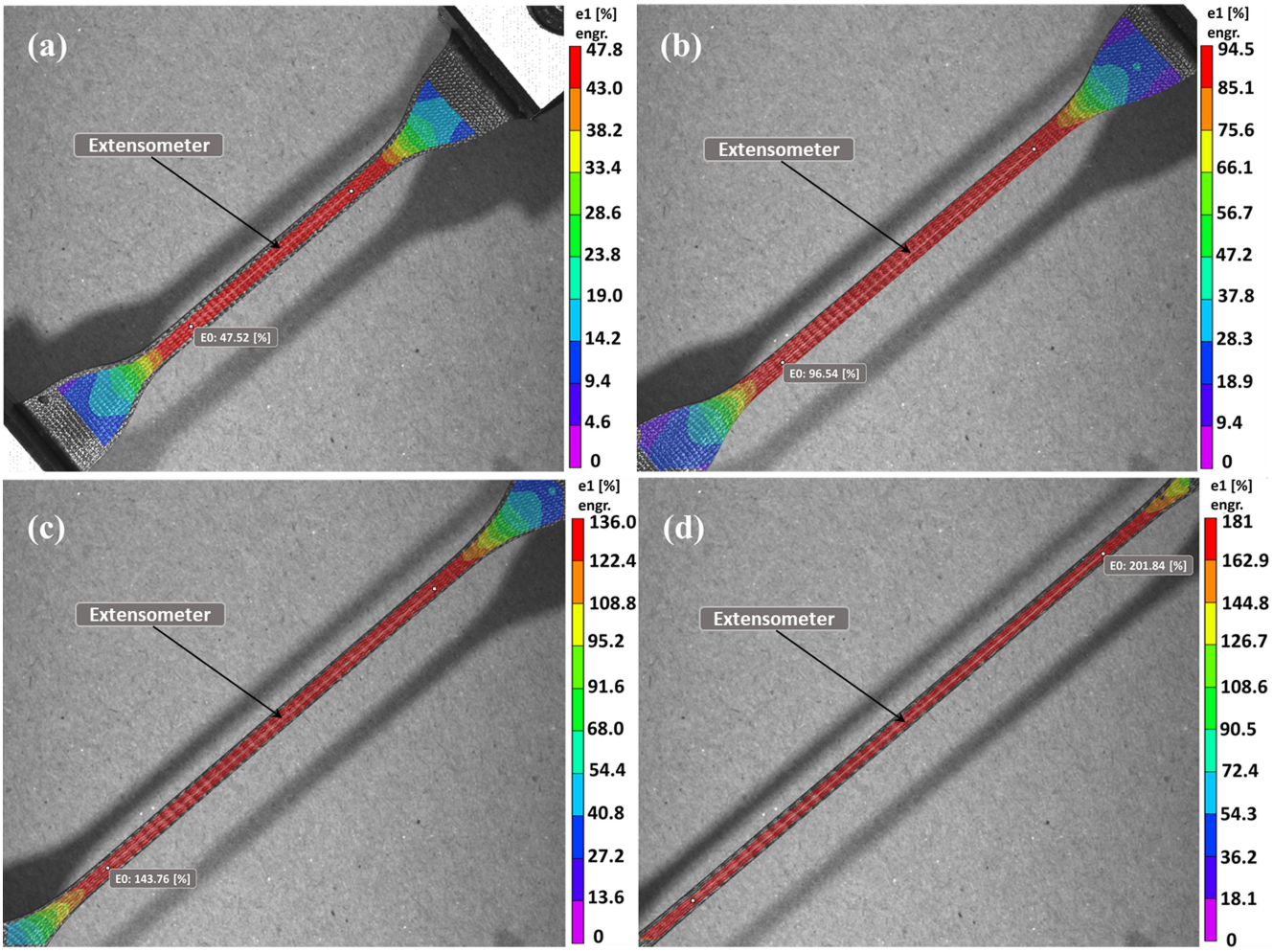

FIGURE 6 | DIC results showing principal strain distribution and nominal strain over the virtual gauge length at maximum displacement: (a) 48% strain, (b) 97% strain, (c) 144% strain, and (d) 202% strain. [Colour figure can be viewed at wileyonlinelibrary.com]

3.3 | Damage Evolution at Macroscale

Figure 8 shows optical images of the fracture surfaces at different perspectives including top and side views to better investigate the damage evolution at the macroscale. It can be concluded that all samples developed a Mode-I fracture (tensile stress normal to the plane of the **crack**) during the fatigue tests, which can be related to the state of loading, i.e., tension-tension mode. In addition, Figure 8a,b,e,f reveal a more deviated crack growth path for samples tested at strains of 48% and 97% in both dry and wet specimens, whereas a further increase of the strain to 202% results in a straighter crack growth path. This can be related to formation of higher crack branching and crack deviations because of the strain amplification and nucleation effects of CNTs into NR when the strain is low [42]. This phenomenon results in an increasing SIC mechanism in front of crack-tips, such that a higher number of crystallites form perpendicular to the crack propagation paths, thus, hampering crack growth and dissipating more energy in the main crack by dividing it into several tiny cracks [42–44]. Unlike this phenomenon observed at a low strain, CNTs cannot effectively hinder crack growth at a higher strain, which results in formation of less SIC arisen from CNTs; thus, a straight crack growth path can be seen as shown in Figure 8c,d,g,h and for both dry and wet samples, respectively. It is worth noting that SIC mechanism in NR typically appears at much higher strain [45]; however, CNTs addition can expedite the nucleation of crystallites in the front of crack-tip at relatively lower strains [42]. Zhan et al. showed that 2% crystallinity at strain of 30% for CNTs/NR, while no crystallites were observed for the neat NR at that strain. In fact, CNTs were considered as nucleation agents resulting in earlier formation of crystallization in the front of the crack-tip originated from polymers chains bonded to them. In other words, further confinements of the molecular chains by CNTs while strained, initiate many precursors lead to the presence of numerous crystallites [46].

Formation of several tiny cracks along the gauge area of dry samples can be accounted for their higher fatigue lives, as shown in Figure 9 . In fact, this is much more notable in the case of 48% strain, manifesting multiple cracks across the gauge zone, as shown in Figure 8a (the cross-sectional image at the stretched condition) and Figure 9. These multiple cracks, called crack lines, are like slip lines that can be observed during plastic deformation in ductile materials. These crack lines are a typical surface morphology that can be seen only for samples possessing ultrahigh fatigue life, 3-phr dry at 48% strain in this study. As a matter of fact, these crack lines cause further energy dissipation over a larger area in the gauge zone rather

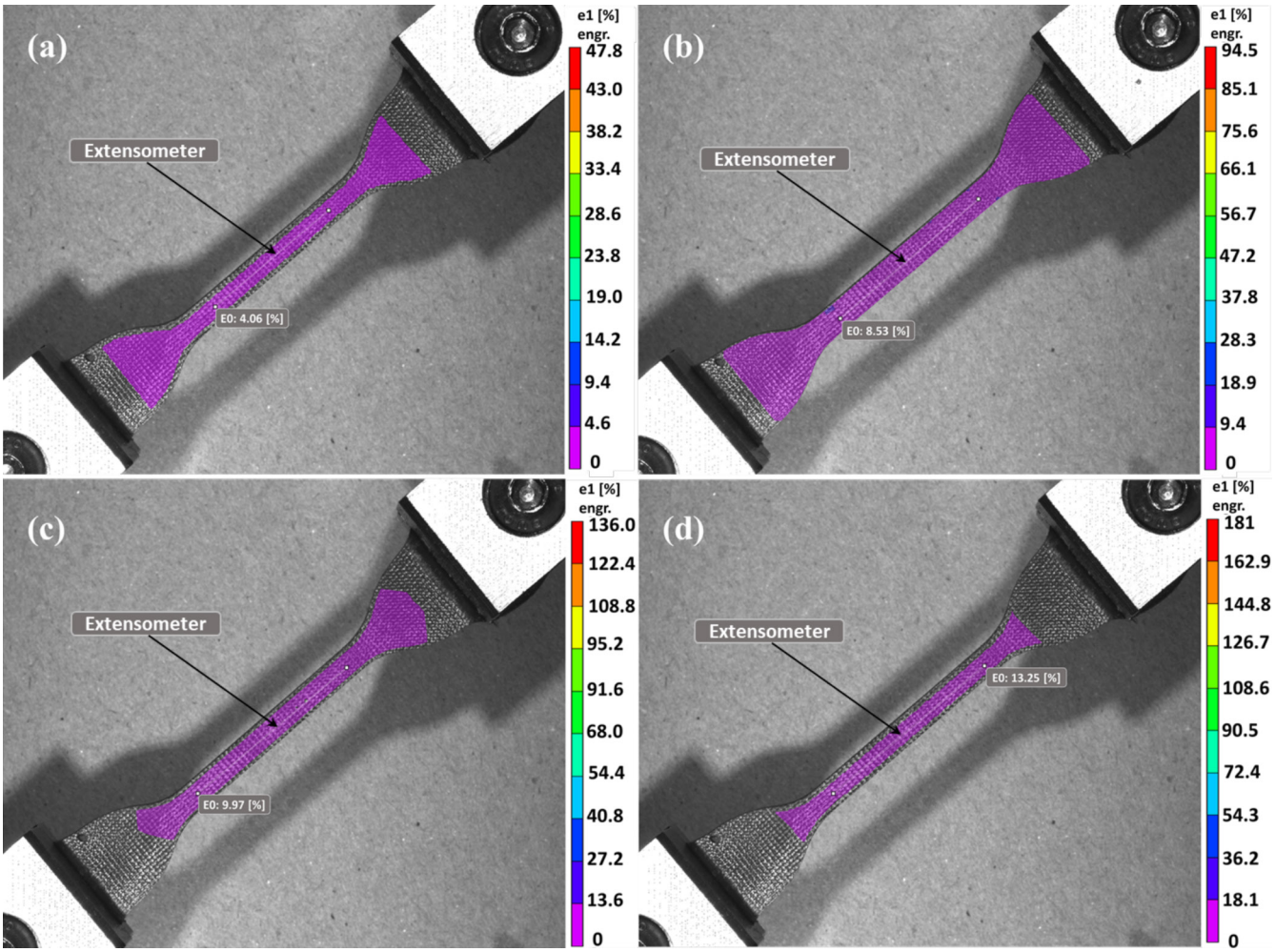

FIGURE 7 | DIC results showing principal strain distribution and nominal strain over the virtual gauge length at minimum displacement: (a) 48% strain, (b) 97% strain, (c) 144% strain, and (d) 202% strain. [Colour figure can be viewed at wileyonlinelibrary.com]

than concentrating the crack-driving force on a few main cracks in the fracture plane; hence, they will contribute significantly to enhancing fatigue life in the case of the dry samples at low strain, i.e., hampering crack growth to the critical length. This indicates that further energy is required to drive the crack growth for the critical crack; thus, a higher fatigue life can be reached. It is worth noting that eventually one main crack in the fracture plane predominates over others and causes fatigue failure. On the contrary, no significant crack lines can be seen in the wet samples at a strain of 48%. In fact, the crack lines are less significant in the case of wet samples, as they contain relatively larger defects requiring less energy to drive their growth due to stress concentration, which results in premature crack growth. Therefore, not only does the density of defects matter, but their geometries and dimensions also play a significant role in quantifying the fatigue life of the NR. This explains the higher fatigue life of dry samples with respect to the wet ones at a macroscale when the strain is low.

The damage evolution during fatigue tests in macroscale is shown in Figure 10. The presence of multiple cracks around the edge of a dog bone specimen is typical in fatigue tests (Figure 10). Two main mechanisms can be taken into account, including crack shielding and crack coalescence. Crack shielding is defined as limiting the growth of tiny cracks in the vicinity of larger cracks (critical ones) as shown by red arrows in Figure 10. The cross-sectional images in unstretched and stretched conditions are provided in Figure 10c, manifesting crack shielding in the vicinity of the failure plane. In fact, parallel arrangements of these multiple tiny cracks play a significant role in enhancing the fatigue life, especially at low strains. In contrast, crack coalescence, accounting for the final stage of fatigue failure, is a phenomenon where a few adjacent cracks merge and create a larger crack, as shown by the green dashed rectangle in Figure 10b. It should be noted that these individual cracks are not necessarily located in the same plane prior to merging. In fact, their orientations are quite different, but they will eventually merge and form a larger crack with critical length in a specific plane, which depends on the specimen boundaries [31]. From a direct observation of the damage evolution during the fatigue test, it can be concluded that a combination of the density of defects within the gauge region, i.e., formation of multiple cracks, far and near the fracture surface, and their further developments via crack shielding and coalescence can be considered for the damage evolution in macroscale [31].

3.4 | Damage Evolution at Microscale

Figure 11 shows SEM images of the fracture surfaces upon fatigue failure for each strain amplitude and compounding

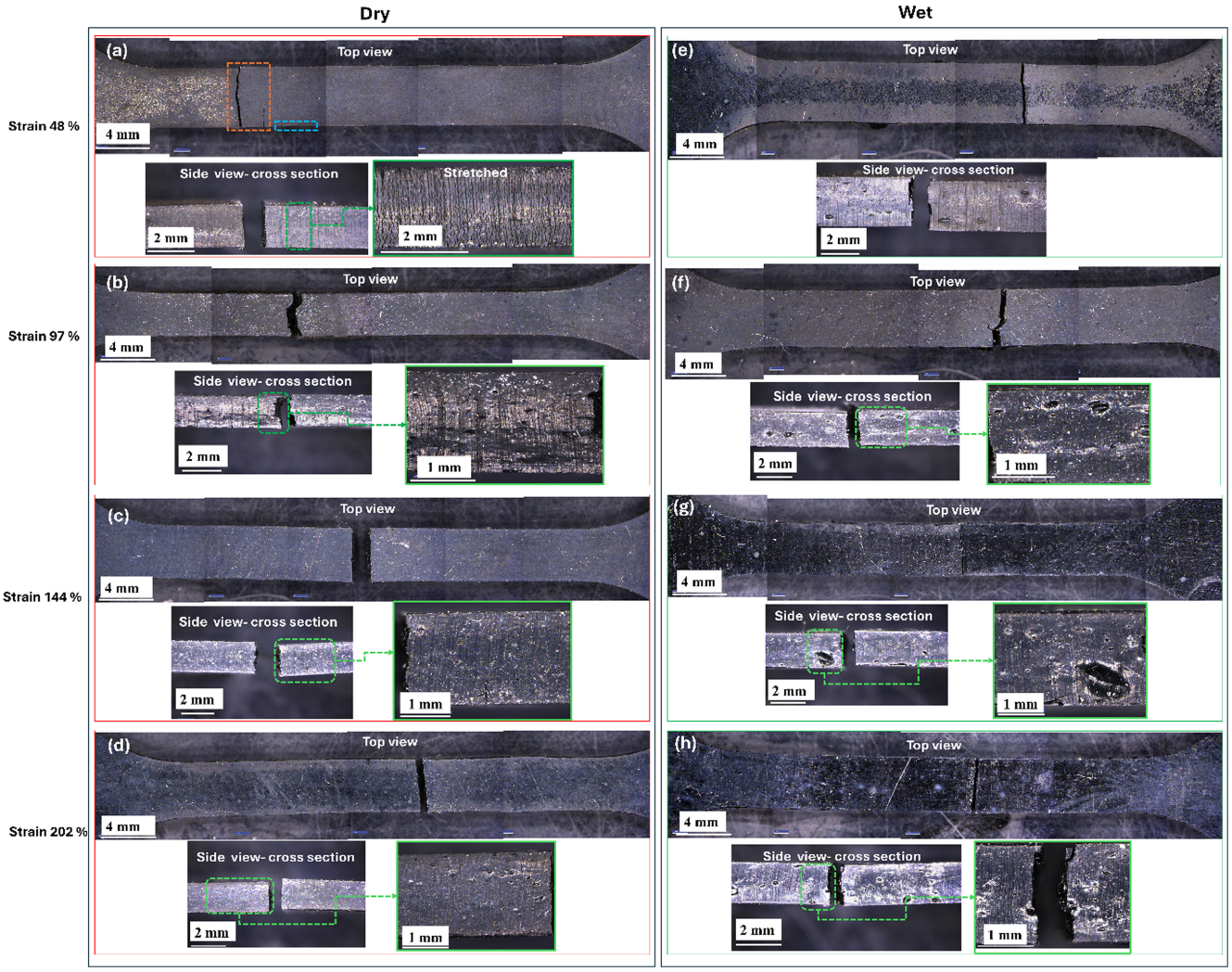

FIGURE 8 | Optical image of the fracture surfaces: (a–d) 3-phr dry at strain of 48%, 97%, 144%, and 202%, respectively, (e–h) 3-phr wet at strain of 48%, 97%, 144%, and 202%, respectively. [Colour figure can be viewed at wileyonlinelibrary.com]

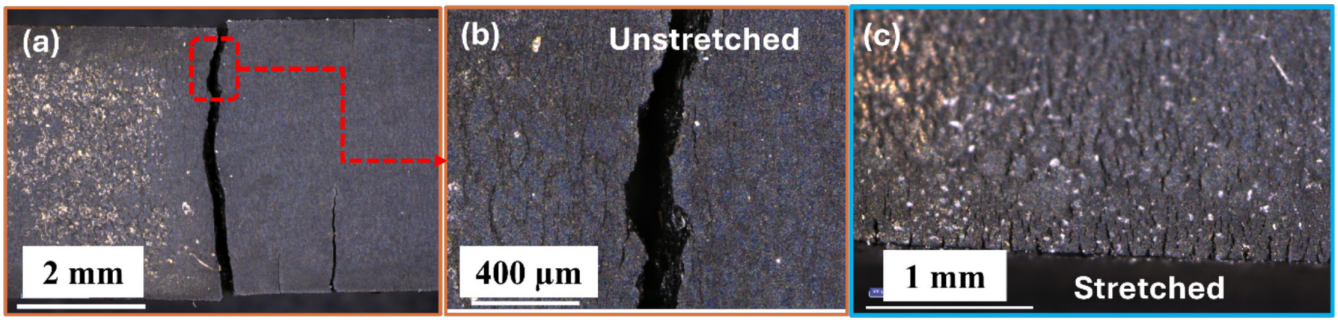

FIGURE 9 | Presence of several crack lines for 3-phr dry at strain of 48% resulting in significant enhancement of the fatigue life: (a,b) higher magnification images corresponding to orange rectangle in Figure 8a, (c) higher magnification image corresponding to blue rectangle in Figure 8a. [Colour figure can be viewed at wileyonlinelibrary.com]

technique. Two different surface morphologies can be distinguished including formation of a rough and smooth-like surfaces corresponding to crack nucleation/stable growth and critical crack growth regions, respectively, as separated by red dashed line in Figure 11. The white dashed arrows in Figure 11a–h demonstrate the critical crack propagation direction. The presence of wrenching and riverlike patterns within the rough and smooth surfaces, respectively, are notable for all samples. The former can be attributed to SIC in NR during the fatigue tests [30, 47], while the latter indicates a more abrupt rupture as manifested by yellow dashed arrows in Figure 10a–h .

Furthermore, several dimples, or cup/cone features, can be seen for both wet and dry samples within rough regions, as

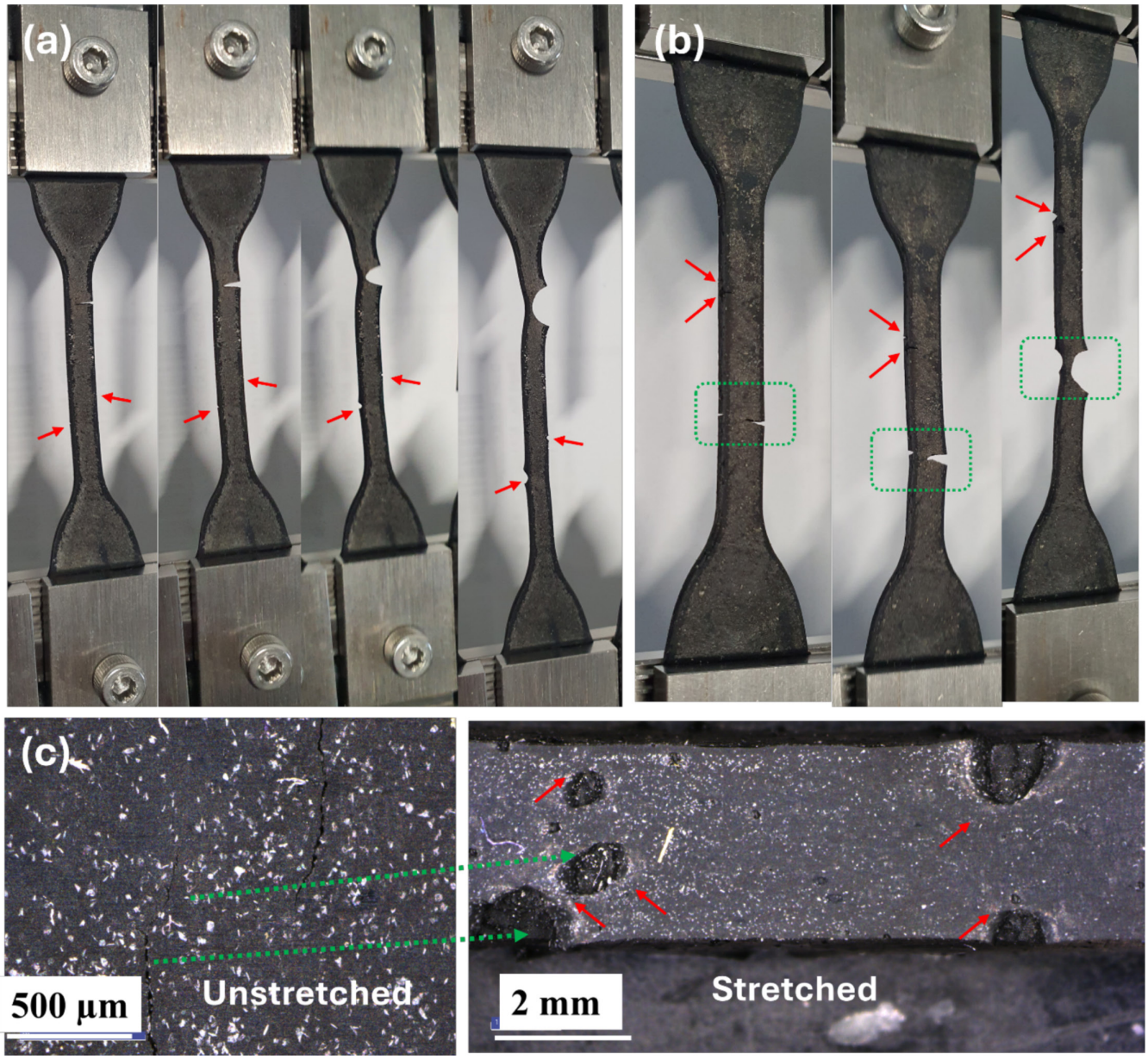

FIGURE 10 | Macroscale damage mechanism in NR-CNT nanocomposites: (a) crack shielding resulting in growth of one critical crack along with presence of multiple cracks in vicinity of the failure plane, (b) a combination of crack shielding and coalescence, (c) crack shielding happening on the cross section. The image is taken from one of the dry samples, but the phenomenon can be observed for both dry and wet samples. Red arrows correspond to crack shielding mechanism. [Colour figure can be viewed at wileyonlinelibrary.com]

highlighted by the dashed red arrows in Figure 11. These features form due to ligament separation, which can be associated with the presence of microvoids. In fact, these dimple structures are formed prior to the macroscopic crack growth resulting from internal defects such as microvoids, which manifest an orientation perpendicular to the stretching direction, surrounded by wrenching patterns, as shown in Figure 11 [30].

Likewise, the area of the rough surface possessing wrenching patterns decreases with an increasing strain, which agrees with the fatigue test findings. This indicates that more energy is dissipated to drive the crack at low strains due to the effective reinforcement of CNTs; thus, a higher number of cycles must be completed for a crack at a specific length to cause failure. It can be concluded that the higher the area of rough surfaces, the higher the fatigue life, as can be seen in Figure 11a,e possessing the highest fatigue life for dry and wet, respectively [10]. It is worth noting that several isolated rough regions appear for 3-phr dry and wet at 97% strain, as shown in Figure 11b,f, respectively. These isolated regions will finally merge into a single crack through crack coalescence, as discussed before, though one predominates the others as they manifest various surface areas [30, 31, 47] .

As mentioned earlier, each crack nucleation site corresponds to a preexisting defect such as voids and CNTs agglomerations. Most samples show a nucleation site at the edge of the sample followed by further 3D propagation until failure, as shown in

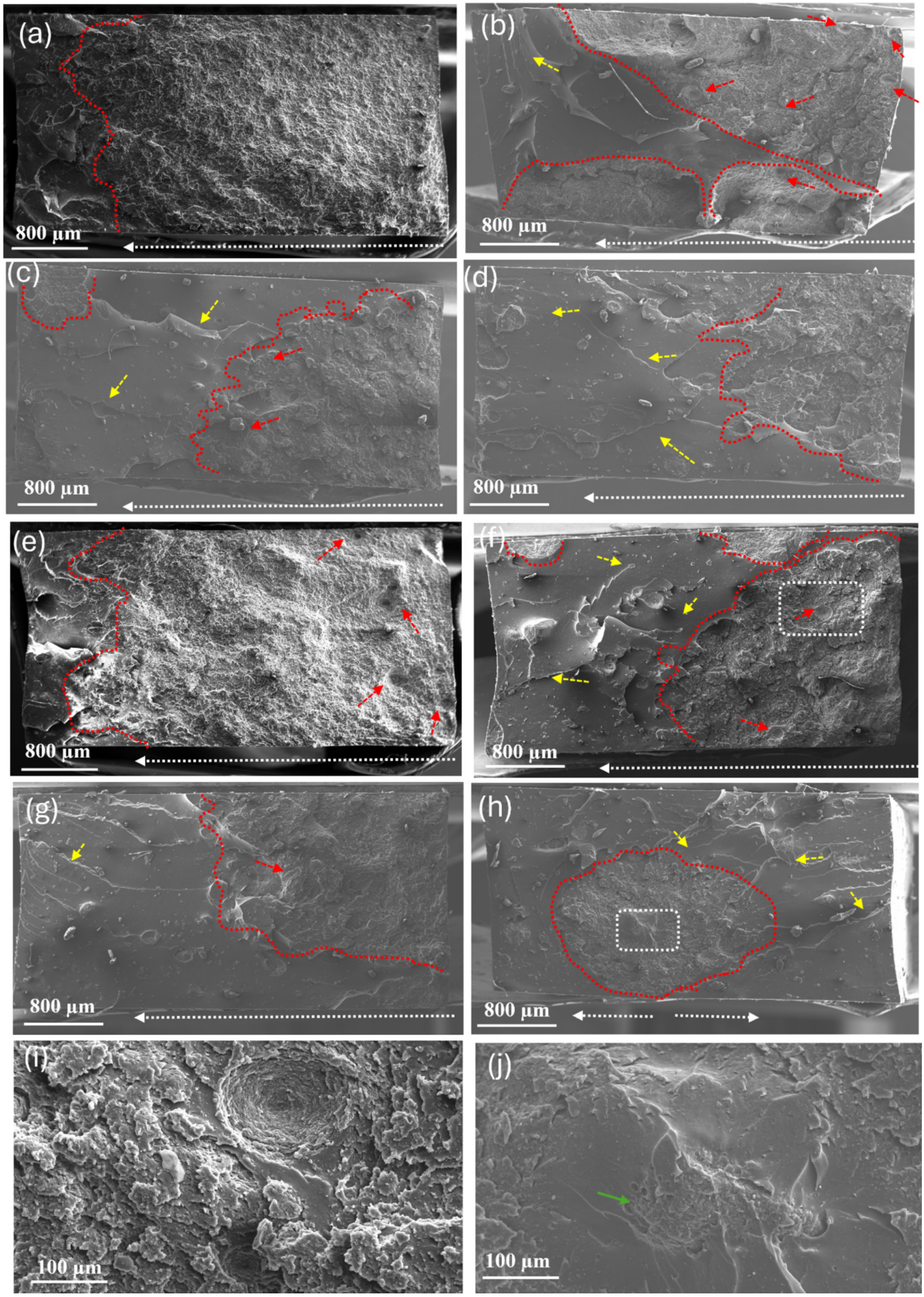

FIGURE 11 | Legend on next page.

FIGURE 11 | SEM image of the fracture surface of samples upon fatigue failure: (a–d) 3-phr dry at strain of 48%, 97%, 144%, and 202%, respectively, (e–h) 3-phr wet at strain of 48%, 97%, 144%, and 202%, respectively, (i,j) higher magnification images corresponding to the white dashed rectangles in (f) and (h), respectively. The white dashed arrows demonstrate the crack propagation direction. The yellow dashed arrows highlight the riverlike patterns while the dashed red arrows indicate presence of dimples, or cup/cone features. [Colour figure can be viewed at wileyonlinelibrary.com]

Figure11a–g, which can be attributed to the presence of voids, as illustrated in Figure 2. In other words, cracks at the edges of specimens exhibit two times the tearing energy versus cracks of the same size in the bulk upon crack opening. In fact, the edge cracks act as if they are twice as large as the bulk cracks, resulting from the free surfaces at the edges behaving as if they are a plane of mirror symmetry [48]. As a result, the critical tear energy can be reached at relatively lower global strains for the edge crack compared to the bulk crack with the same length, making it the more likely failure point [48]. This explains why most failures occur at the edge of specimens both for the fatigue and monotonic stress–strain to break tests [48]. In contrast, an internal nucleation site can be seen for a few samples, especially at high strains, as shown in Figure 11h,i, which can be related to the presence of CNTs agglomeration accompanied by voids. From Figure 11i, it can be concluded that damage evolution in situ internal defect is quite different, i.e., upon the crack nucleation, a riverlike pattern or striation can be seen around the nucleation site followed by a rough surface resulting from high local crystallinity [30] and eventually final rupture manifesting a smooth surface again.

4 | Conclusion

CNTs incorporation into NR, as one of the promising nanofillers in tailoring mechanical properties of rubbers, was investigated by performing fatigue tests on samples prepared by wet and dry techniques. In summary, the following outcomes can be drawn:

- Wet approach possessed higher numbers of large defects such as voids and higher surface roughness in contrast to the dry approach resulting from higher amounts of entrapped air and aggregation of randomly dispersed nonrubber particles including non-insoluble hydrophilic proteins and phospholipids in toluene within the rubber matrix.
- Wet materials possessed more homogeneous CNTs dispersion, whereas the presence of CNT agglomerations accompanied with CNTs-poor regions was more pronounced in the dry method.
- Mullins effect and permanent set were observed for both dry and wet samples resulting from the breakage of CNTs' networks as well as CNTs/rubber interactions, while no considerable difference in the hysteresis was noted among them.
- A maximum average fatigue life of 1.58 and 1.09 million cycles, respectively, at 48% strain was achieved for dry and wet. In total, dry samples possessed a higher fatigue life compared to the wet samples at all strain amplitudes due to a smaller number of flaws. The presence of relatively higher numbers of large defects including voids in the wet batch accounted for a significant reduction of the fatigue life.
- Crack branching and crack deviations were accounted for more deviated crack growth paths for fatigue tests conducted at strains of 48% and 97% in both dry and wet specimens. In contrast, a straighter crack propagation was observed at larger strains, indicating CNTs were less effective at higher strains.
- Further energy dissipation over a larger area in the gauge zone resulting from the formation of multiple tiny cracks, especially at low strains, instead of accumulating crack-driving force into one individual crack, contributed to enhancing the fatigue life of the dry samples. In contrast, only a few minor cracks evolved in the wet samples throughout fatigue tests due to a relatively higher number of large pre-existing defects acting as stress concentrators, which led to premature crack growth.
- Damage evolution mechanisms at macroscale were defined as crack shielding and crack coalescence. A combination of the density of flaws across the gauge region, i.e., the occurrence of multiple cracks and their further developments via crack shielding and crack coalescence can be considered for the damage evolution in macroscale.
- Damage evolution in microscale showed the presence of wrenching and riverlike patterns on fractured surfaces. The former was attributed to the SIC in NR during fatigue tests, whereas the latter referred to a more abrupt rupture.
- It was concluded that the dry approach can be a better approach with respect to the wet technique considering quasi-static and fatigue properties, the environmental concerns of using solvent, and cost. Therefore, depending on the end user application, one might select the proper CNTs dispersion technique; the wet approach is more in favor of enhancing quasi-static properties, while the dry one can be the ideal choice for achieving better repeated cyclic properties such as fatigue life. For instance, fatigue life is of importance for WECs where NR is used as a flexible membrane; therefore, the dry method can be a superior approach in CNT/NR compounding for the aforementioned application.

Author Contributions

Ali Esmaeili: conceptualization, methodology, investigation, experiment, initial draft, writing and editing, and data analysis. **Deepak George:** experiment, reviewing and editing, and data analysis. **Thomas Lake:** reviewing and editing and data analysis. **Lewis Tunnicliffe:** reviewing and editing and data analysis. **Ian Masters:** reviewing and editing and data analysis. **Mokarram Hossain:** conceptualization, grant management, writing and editing, and data analysis.

Acknowledgments

This study is funded by the Swansea Bay City Deal and the European Regional Development Fund through the Welsh European Funding Office. This study is also supported by EPSRC through the Supergen ORE Hub (EP/S000747/1), who have awarded funding for the Flexible Fund project Supergen ORE Hub Flexible Fund (FF2021-1036). Ali Esameili and Mokarram Hossain acknowledge the financial support from Birla Carbon (USA) to facilitate parts of this study. We would like to thank the access to characterization equipment to Swansea University Advanced Imaging of Materials (AIM) facility, which was funded in part by the EPSRC (EP/M028267/1) and the European Regional Development Fund through the Welsh Government (80708). Mokarram Hossain also acknowledges the support of the EPSRC via a Standard Grant (EP/Z535710/1) and the Royal Society (UK) through the International Exchange Grant (IEC/NSFC/211316). We would like to thank Dr. Christian Hacker for performing the transmission electron microscopy (TEM) for this project at the Bioimaging Centre, University of Exeter.

Data Availability Statement

The data that supports the findings of this study are available in the supplementary material of this article

References

1. S. Ning, B. Su, S. Liu, et al., "Failure Behaviors of Cord-Rubber Composite Materials Under Mixed Mode I/II Loading: Experimental and Numerical Simulation," *Materials Today Communications* 41 (2024): 110349, https://doi.org/10.1016/j.mtcomm.2024.110349.

2. I. Collins, M. Hossain, W. Dettmer, and I. Masters, "Flexible Membrane Structures for Wave Energy Harvesting: A Review of the Developments, Materials and Computational Modelling Approaches," *Renewable and Sustainable Energy Reviews* 151 (2021): 111478, https://doi.org/10.1016/j.rser.2021.111478.

3. A. Esmaeili, D. George, I. Masters, and M. Hossain, "Biaxial Experimental Characterizations of Soft Polymers: A Critical Review," *Polymer Testing* 128 (2023): 108246, https://doi.org/10.1016/j.polymertesting.2023.108246.

4. A. Esmaeili, M. Hossain, and I. Masters, "Comparison of Two Compounding Techniques for Carbon Nanotubes Filled Natural Rubbers Through Microscopic and Dynamic Mechanical Characterizations," *Materials Letters* 335 (2023): 133786, https://doi.org/10.1016/j.matlet.2022.133786.

5. R. J. Harbour, A. Fatemi, and W. V. Mars, "Fatigue Crack Growth of Filled Rubber Under Constant and Variable Amplitude Loading Conditions," *Fatigue & Fracture of Engineering Materials & Structures* 30 (2007): 640–652, https://doi.org/10.1111/j.1460-2695.2007.01143.x.

6. K. Głowacka, J. Klemenc, M. Nagode, and T. Łagoda, "Fatigue Lifetime of Rubber Composites—State-of-the-Art," *Polymer Testing* 143 (2025): 108713, https://doi.org/10.1016/j.polymertesting.2025.108713.

7. P. C. O. Adu, M. Aakyiir, X. Su, et al., "Challenges and Advancements in Elastomer/CNT Nanocomposites With Mechanochemical Treatment, Reinforcement Mechanisms and Applications," *Smart Materials in Manufacturing* 2 (2024): 100053, https://doi.org/10.1016/j.smmf.2024.100053.

8. H. Guo, S. Jerrams, Z. Xu, et al., "Enhanced Fatigue and Durability of Carbon Black/Natural Rubber Composites Reinforced With Graphene Oxide and Carbon Nanotubes," *Engineering Fracture Mechanics* 223 (2020): 106764, https://doi.org/10.1016/j.engfracmech.2019.106764.

9. X. Ji, X. Zhang, J. Yue, Y. Lu, and L. Zhang, "Comparative Study on the Effect of Carbon Nanotubes and Carbon Black on Fatigue Properties of Natural Rubber Composites," *International Journal of Fatigue* 163 (2022): 107094, https://doi.org/10.1016/j.ijfatigue.2022.107094.

10. Y. Ding, X. Cao, G. Weng, Q. Yin, L. Wang, and Z. Chen, "Crack Growth Behavior of Natural Rubber Influenced by Functionalized Carbon Nanotubes," *Journal of Applied Polymer Science* 134 (2017): 2–9, https://doi.org/10.1002/app.44527.

11. B. Dong, L. Zhang, and Y. Wu, "Influences of Different Dimensional Carbon-Based Nanofillers on Fracture and Fatigue Resistance of Natural Rubber Composites," *Polymer Testing* 63 (2017): 281–288, https://doi.org/10.1016/j.polymertesting.2017.08.035.

12. X. Wang, Z. Liu, X. Zeng, and Y. Xu, "A Method to Obtain Probabilistic Fatigue Lives Under Varying Strain Peaks for Rubber Components With Small Samples," *Fatigue & Fracture of Engineering Materials & Structures* 47 (2024): 2955–2968, https://doi.org/10.1111/ffe.14356.

13. F. Nargesi Azam, M. Alimardani, and S. Shokoohi, "Thermal and Fatigue Failure Properties of Graphene Oxide/Acrylonitrile Butadiene Rubber Composites: New Perspectives on the Role of Interface and Interphase," *Polymer Composites* 46, no. 10 (2025): 1–9020, https://doi.org/10.1002/pc.29536.

14. R. Barbosa, R. Gonçalves, K. A. Tozzi, M. C. Saccardo, A. G. Zuquello, and C. H. Scuracchio, "Improving the Swelling, Mechanical, and Electrical Properties in Natural Rubber Latex/Carbon Nanotubes Nanocomposites: Effect of the Sonication Method," *Journal of Applied Polymer Science* 139 (2022): e5232, https://doi.org/10.1002/app.52325.

15. A. A. Abdullateef, S. P. Thomas, M. A. Al-Harthi, et al., "Natural Rubber Nanocomposites With Functionalized Carbon Nanotubes: Mechanical, Dynamic Mechanical, and Morphology Studies," *Journal of Applied Polymer Science* 125 (2012): E76–E84, https://doi.org/10.1002/app.35021.

16. P. S. Thomas, A. A. Abdullateef, M. A. Al-Harthi, et al., "Electrical Properties of Natural Rubber Nanocomposites: Effect of 1-Octadecanol Functionalization of Carbon Nanotubes," *Journal of Materials Science* 47 (2012): 3344–3349, https://doi.org/10.1007/s10853-011-6174-4.

17. K. Kueseng and K. I. Jacob, "Natural Rubber Nanocomposites With SiC Nanoparticles and Carbon Nanotubes," *European Polymer Journal* 42 (2006): 220–227, https://doi.org/10.1016/j.eurpolymj.2005.05.011.

18. A. Esmaeili, I. Masters, and M. Hossain, "A Novel Carbon Nanotubes Doped Natural Rubber Nanocomposite With Balanced Dynamic Shear Properties and Energy Dissipation for Wave Energy Applications," *Results in Materials* 17 (2023): 100358, https://doi.org/10.1016/j.rinma.2022.100358.

19. W. V. Mars and A. Fatemi, "A Literature Survey on Fatigue Analysis Approaches for Rubber," *International Journal of Fatigue* 24 (2002): 949–961, https://doi.org/10.1016/S0142-1123(02)00008-7.

20. Y. L. Tee, M. S. Loo, and A. Andriyana, "Recent Advances on Fatigue of Rubber After the Literature Survey by Mars and Fatemi in 2002 and 2004," *International Journal of Fatigue* 110 (2018): 115–129, https://doi.org/10.1016/j.ijfatigue.2018.01.007.

21. L. B. Tunnicliffe, "Fatigue Crack Growth Behavior of Carbon Black-Reinforced Natural Rubber," *Rubber Chemistry and Technology* 94 (2021): 494–514, https://doi.org/10.5254/RCT.21.79935.

22. J. Rong, J. Yang, Y. Huang, W. Luo, and X. Hu, "Characteristic Tearing Energy and Fatigue Crack Propagation of Filled Natural Rubber," *Polymers (Basel)* 13 (2021): 2–11, https://doi.org/10.3390/polym13223891.

23. T. Kocjan, M. Nagode, J. Klemenc, and S. Oman, "On Fatigue Crack Growth Testing and Analysis of Non-Crystallising Rubber Using Planar Tension Specimen," *Polymer Testing* 117 (2023): 107819, https://doi.org/10.1016/j.polymertesting.2022.107819.

24. C. Xue, H. Gao, and G. Hu, "Viscoelastic and Fatigue Properties of Graphene and Carbon Black Hybrid Structure Filled Natural Rubber Composites Under Alternating Loading," *Construction and Building Materials* 265 (2020): 120299, https://doi.org/10.1016/j.conbuildmat.2020.120299.

25. F. Stadlbauer, T. Koch, F. Planitzer, W. Fidi, and V. M. Archodoulaki, "Setup for Evaluation of Fatigue Crack Growth in Rubber: Pure Shear Sample Geometries Tested in Tension-Compression Mode," *Polymer Testing* 32 (2013): 1045–1051, https://doi.org/10.1016/j.polymertesting.2013.06.003.

26. A. Zine, N. Benseddiq, M. Nait-Abdelaziz, and N. Ait Hocine, "Prediction of Rubber Fatigue Life Under Multiaxial Loading," in *Fracture of Nano and Engineering Materials and Structures*, ed. E. E. Gdoutos (Springer, 2006), https://doi.org/10.1007/1-4020-4972-2_380.

27. J. B. Le Cam, B. Huneau, and E. Verron, "Fatigue Damage in Carbon Black Filled Natural Rubber Under Uni- and Multiaxial Loading Conditions," *International Journal of Fatigue* 52 (2013): 82–94, https://doi.org/10.1016/j.ijfatigue.2013.02.022.

28. W. B. Shangguan, X. L. Wang, J. X. Deng, S. Rakheja, X. Y. Pan, and B. Yu, "Experiment and Modeling of Uniaxial Tension Fatigue Performances for Filled Natural Rubbers," *Materials and Design* 58 (2014): 65–73, https://doi.org/10.1016/j.matdes.2014.01.035.

29. P. Y. Le Gac, M. Arhant, P. Davies, and A. Muhr, "Fatigue Behavior of Natural Rubber in Marine Environment: Comparison Between Air and Sea Water," *Materials and Design* 65 (2015): 462–467, https://doi.org/10.1016/j.matdes.2014.09.032.

30. B. Ruellan, J. B. Le Cam, I. Jeanneau, F. Canévet, F. Mortier, and E. Robin, "Fatigue of Natural Rubber Under Different Temperatures," *International Journal of Fatigue* 124 (2019): 544–557, https://doi.org/10.1016/j.ijfatigue.2018.10.009.

31. W. V. Mars and A. Fatemi, "Nucleation and Growth of Small Fatigue Cracks in Filled Natural Rubber Under Multiaxial Loading," *Journal of Materials Science* 41 (2006): 7324–7332, https://doi.org/10.1007/s10853-006-0962-2.

32. W. V. Mars and A. Fatemi, "Fatigue Crack Nucleation and Growth in Filled Natural Rubber," *Fatigue & Fracture of Engineering Materials & Structures* 26 (2003): 779–789, https://doi.org/10.1046/j.1460-2695.2003.00678.x.

33. S. Echchur Rangarajan and K. K. Ramarathnam, "Damage Evolution in Natural Rubber: An Experimental Study," *Journal of the Mechanics and Physics of Solids* 137 (2020): 103850, https://doi.org/10.1016/j.jmps.2019.103850.

34. F. E. Ngolemasango, G. E. Nkeng, C. O'Connor, J. Manley, M. Bennett, and J. Clarke, "Effect of Nature and Type of Flaw on the Properties of a Natural Rubber Compound," *Polymer Testing* 28 (2009): 463–469, https://doi.org/10.1016/j.polymertesting.2009.02.007.

35. P. Rojruthai, J. Sakdapipanich, J. Wiriyanantawong, C. C. Ho, and N. Chaiear, "Effect of Latex Purification and Accelerator Types on Rubber Allergens Prevalent in Sulphur Prevulcanized Natural Rubber Latex: Potential Application for Allergy-Free Natural Rubber Gloves," *Polymers (Basel)* 14 (2022): 4679, https://doi.org/10.3390/polym14214679.

36. R. J. Harbour, A. Fatemi, and W. V. Mars, "Fatigue Crack Orientation in NR and SBR Under Variable Amplitude and Multiaxial Loading Conditions," *Journal of Materials Science* 43 (2008): 1783–1794, https://doi.org/10.1007/s10853-007-2398-8.

37. M. Sriring, A. Nimpaiboon, S. Kumarn, et al., "Film Formation Process of Natural Rubber Latex Particles: Roles of the Particle Size and Distribution of Non-Rubber Species on Film Microstructure," *Colloids and Surfaces A: Physicochemical and Engineering Aspects* 592 (2020): 124571, https://doi.org/10.1016/j.colsurfa.2020.124571.

38. L. C. Tang, L. Zhao, F. Qiang, Q. Wu, L. X. Gong, and J. P. Peng, *Mechanical Properties of Rubber Nanocomposites Containing Carbon Nanofillers* (Elsevier Inc., 2019), https://doi.org/10.1016/B978-0-12-817342-8.00012-3.

39. C. G. Robertson, L. B. Tunnicliffe, L. Maciag, et al., "Characterizing Distributions of Tensile Strength and Crack Precursor Size to Evaluate Filler Dispersion Effects and Reliability of Rubber," *Polymers (Basel)* 12 (2020): 203, https://doi.org/10.3390/polym12010203.

40. H. Huang, Z. Wang, C. Dai, J. Guo, and X. Zhang, "Volatile Organic Compounds Emission in the Rubber Products Manufacturing Processes," *Environmental Research* 212 (2022): 113485, https://doi.org/10.1016/j.envres.2022.113485.

41. A. N. Gent, *Engineering With Rubber: How to Design Rubber Components*, 3rd ed. Revised Edition (Carl Hanser Verlag GmbH & Co. KG, 2012).

42. Y. Zhan, N. Yan, G. Fei, H. Xia, and Y. Meng, "Crack Growth Resistance of Natural Rubber Reinforced With Carbon Nanotubes," *Journal of Applied Polymer Science* 137 (2020): 1–9, https://doi.org/10.1002/app.48447.

43. G. H. Chen Xue and H. Gao, "Enhanced Fatigue and Durability of Carbon Black/Natural Rubber Composites Reinforced With Graphene Oxide and Carbon Nanotubes," *International Journal of Fatigue* 335 (2020): 133786, https://doi.org/10.1016/j.matlet.2022.133786.

44. H. Guo, P. Ji, I. Z. Halász, et al., "Enhanced Fatigue and Durability Properties of Natural Rubber Composites Reinforced With Carbon Nanotubes and Graphene Oxide," *Materials (Basel)* 13 (2020): 1–12, https://doi.org/10.3390/ma13245746.

45. B. Huneau, "Strain-Induced Crystallization of Natural Rubber: A Review of X-Ray Diffraction Investigations to Cite This Version: HAL Id: hal-01007326 Strain-Induced Crystallization of Natural Rubber: A Review of X-Ray Diffraction Investigations," *Rubber Chemistry and Technology* 84 (2011): 425–452.

46. Y. Nie, Z. Gu, Y. Wei, T. Hao, and Z. Zhou, "Features of Strain-Induced Crystallization of Natural Rubber Revealed by Experiments and Simulations," *Polymer Journal* 49 (2017): 309–317, https://doi.org/10.1038/pj.2016.114.

47. J. Le Cam, B. Huneau, E. Verron, and L. Gornet, "Mechanism of Fatigue Crack Growth in Carbon Black Filled Natural Rubber," *Macromolecules* 37 (2004): 5011–5017.

48. L. B. Tunnicliffe, C. G. Robertson, and W. V. Mars, "A Microscopy Investigation of Rubber Compound Crack Precursors and Tensile Fracture Surfaces," *Rubber Chemistry and Technology* 96 (2023): 514–529, https://doi.org/10.5254/rct-23.201163.

Supporting Information

Additional supporting information can be found online in the Supporting Information section. **Video S1:** Supplementary video. **Video S2:** Supplementary video. **Video S3:** Supplementary video. **Video S4:** Supplementary video.